



1 Reliability Analysis Method for Soil Slopes Permanent
2 Displacement under Mainshock-Aftershock Sequences

3 Tianyi Wang ^{a, b}, Chengda Zhang ^{c*}, Jiangwei Zhang ^{d*}, Su Chen ^e, Zhijun Dai ^{f*}

4 a. Key Laboratory of Intelligent Detection and Equipment for Underground Space of Beijing-Tianjin-Hebei Urban Agglomeration, Ministry of Natural
5 Resources, Hebei GEO University, Shijiazhuang, 050031, China;
6 b. College of Earth Sciences, Hebei GEO University, Shijiazhuang, 050031, China;
7 c. 519 Team of North China Geological Exploration Bureau, Tianjin North China Geological Exploration Bureau, Baoding 071051, China;
8 d. State Key Laboratory of Hydrosience and Engineering, Tsinghua University, Beijing 100084, China;
9 e. Institute of Geophysics, China Earthquake Administration, Beijing 100081, China;
10 f. Key Laboratory of Urban Security and Disaster Engineering of the Ministry of Education, Beijing University of Technology, Beijing 100124, China.
11 **Correspondence:** Chengda Zhang (zcd_geo@163.com), Jiangwei Zhang (zhangjiangwei@tsinghua.edu.cn) and Zhijun Dai(dzi@cea-igp.ac.cn)

12 **Abstract**

13 After a primary seismic event, subsequent aftershocks frequently induce progressive damage to
14 slopes. Evaluating the response of slopes to mainshock-aftershock sequence (MAS) from a
15 probabilistic perspective is crucial for disaster prevention and mitigation. Current research primarily
16 focuses on single mainshock events, with limited consideration of the aftershock effects. Our study
17 addresses the MAS events. Firstly, the random input field of the MAS is constructed through the
18 collaboration of theoretical models and real data. Then, considering the peak characteristics,
19 cumulative characteristics and spectral characteristics of the MAS, the numerical simulation method
20 is used to explore the control parameters for the soil slope response. Ultimately, leveraging the
21 probability density evolution method (PDEM), we introduce a reliability assessment framework for
22 soil slope behavior under MAS loading. Compared with the existing approaches, the new method
23 fully accounts for aftershock characteristics and assesses the degree of slope permanent
24 displacement response with greater precision. These results offer substantial practical utility for
25 engineering applications and serve as guidance for slope stability assessment and disaster mitigation
26 strategies.

27 **Keywords:** mainshock-aftershock sequences, probability density evolution method, seismic
28 response, soil slope, permanent displacement reliability

29 **1 Introduction**

30 Strong seismic events generally trigger subsequent smaller earthquakes. The impact of
31 aftershocks on slopes cannot be ignored, as they may trigger more severe incremental damage
32 effects (Yin et al, 2023). As safety requirements for engineering structures continue to escalate,
33 slope stability under MAS has attracted considerable interest from researchers and practitioners
34 alike. Li et al. (2009, 2017) pioneered and refined the PDEM framework for examining stochastic
35 dynamic systems, establishing novel methodologies for nonlinear stochastic dynamic analysis and
36 reliability evaluation of large-scale complex engineering structures. This framework demonstrates
37 particular effectiveness when applied to slope stochastic dynamic investigations. Expanding upon
38 this foundation, Pang et al. (2021, 2024) introduced an enhanced generalized-PDEM approach for
39 examining reliability in complex slope configurations. Their methodology encompasses multiple

* Corresponding author.

E-mail addresses: zhangjiangwei@mail.tsinghua.edu.cn (J. Zhang), zcd_geo@163.com (C. Zhang), dzi@cea-igp.ac.cn (Z. Dai), chensuchina@126.com (S. Chen).



40 slope parameters alongside ground motion uncertainties. Additionally, accounting for the spatial
 41 variation in soil strength properties, a reliability assessment methodology integrating the Newmark
 42 method and PDEM is developed to evaluate the effects of aftershocks and spatial heterogeneity on
 43 slope dynamic reliability. (Zhou et al., 2023; Wang et al., 2023; Xu et al., 2025). Contemporary
 44 investigations predominantly utilize peak ground acceleration (PGA) as the primary intensity metric.
 45 Nevertheless, within MAS contexts, maximum PGA typically manifests during the mainshock
 46 phase. Consequently, intensity parameters derived solely from peak values inadequately
 47 characterize the comprehensive ground motion attributes of MAS. (Ruiz-Garcia and Negrete-
 48 Manriquez 2011; Amiri et al., 2022).

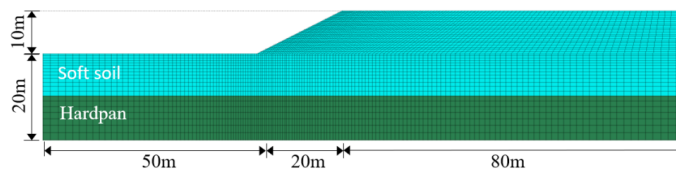
49 In terms of characterizing the ground motion random field of the MAS, the Monte Carlo method
 50 is a classic and effective means (Hu et al., 2018; Nithin et al., 2020; Kim and Sitar, 2013). However,
 51 it also has problems such as a large number of samples and incomplete probability information of
 52 the sample set (Jiang et al., 2021). Since the MAS time histories obtained via the random function
 53 - dimension reduction simulation technique carries associated probabilities and establish a complete
 54 probabilistic set, they can be coupled with PDEM to perform sophisticated dynamic response and
 55 reliability analyses for complex engineering structures under MAS excitation. (Liu et al., 2017; Liu
 56 et al., 2019; Liu et al., 2022).

57 Considering the peak value, cumulative and spectral characteristics of MAS, a slope reliability
 58 analysis method is proposed, adeptly accounting for the characteristics of the aftershock. The
 59 findings offer a reference for stability evaluation and disaster prevention of soil slopes under MAS
 60 ground motions.

61 2 Methods

62 2.1 Model

63 This investigation employs a binary structural slope configuration to examine slope under the
 64 MAS. Fig. 1 shows the double-layer slope model established by referring to Wang et al. (2022). The
 65 dimensions of the model are 150 m in length and 30 m in height. Grid dimensions ΔL range from
 66 0.5 m to 1.8 m, with a finer resolution of approximately 0.5 m in the potential sliding zone. The soil
 67 material is clay sourced from the southwestern region of China (Yang et al., 2022; Ma et al., 2023;
 68 Zhang et al., 2024), and its properties are detailed in Table 1.



69
70
71 **Fig. 1.** Geometric dimensions and mesh division of the slope model

Table 1 Parameters of the slope

Soil layer	Density / ($\text{kg}\cdot\text{m}^{-3}$)	Bulk modulus /MPa	Shear modulus /MPa	Cohesion /kPa	Internal friction angle /($^{\circ}$)	Shear strength /kPa
Soft soil	1900	70	37	34	24	4.2
Hardpan	2000	875	560	120	42	120

72



73 This investigation utilizes the finite-difference platform FLAC3D, with soil mechanical behavior
74 characterized through a Mohr-Coulomb constitutive formulation incorporating tensile-cutoff provisions.
75 Local damping is adopted in this study. Its implementation is given by Ep. (1) (Li et al., 2006). Given
76 that this computational strategy eliminates the requirement for global matrix construction, substantial
77 reductions in time step magnitudes become achievable. Such computational architecture enhances
78 processing efficiency without compromising solution fidelity, rendering this methodology particularly
79 appropriate for investigating nonlinear dynamic phenomena. (Hu et al., 2017; Puthanpurayil et al., 2018;
80 Yan et al., 2011).

$$81 \quad \xi = \pi D_s \quad (1)$$

82 Within Equation (1), the coefficient ξ quantifies localized damping intensity, D_s designates the
83 critical damping fraction, while π maintains its conventional value of 3.14.

84 This investigation adopts a 5% critical damping fraction to replicate energy dissipation characteristics
85 during seismic wave transmission through soil media (Qu et al., 2015), yielding a local damping
86 coefficient of 0.157 according to Ep. (1).

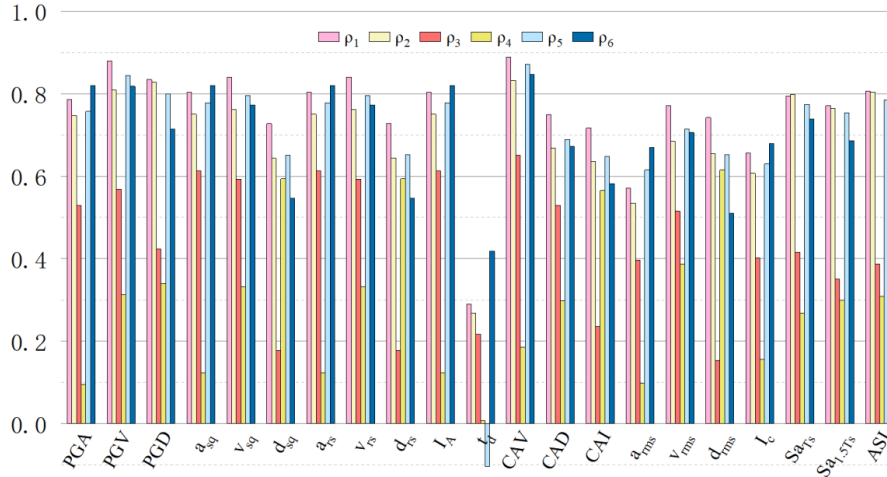
87 **2.2 Reliability analysis method of slope under MAS**

88 Leveraging fundamental probability conservation principles, we may derive generalized density
89 evolution equations applicable to stochastic dynamic system investigations. Integration with virtual
90 stochastic process methodologies facilitates probabilistic modeling of stochastic datasets.
91 Furthermore, based on the PDEM, the reliability analysis of the permanent displacement of the slope
92 under the MAS action is realized (Li et al., 2008; Liu et al., 2017; Jiang et al., 2021). The main steps
93 are as follows:

94 (1) The measured data of the MAS were statistically analyzed to obtain the frequency-domain
95 energy distribution function curves of each ground motion. Employing optimal square
96 approximation criteria, we determine the parameter vector λ defining each evolving power spectral
97 density function. The seismic in Section 3 can be regarded as a zero-mean non-stationary ground
98 motion process generated by the evolving power spectral density function model. The discrete
99 representative points of each ground motion are expressed as $\theta_q = (\theta_{1,q}, \theta_{2,q}, \dots, \theta_{s,q}, q = 1, 2, \dots,$
100 $96)$, the discrete representative points assigned to probability for Eq. (2) :

$$101 \quad P_q = \int_{V_q} p\theta(\theta) d\theta \quad (2)$$

102 (2) Previous research by our group demonstrated that among the 21 parameters evaluated across
103 three categories—namely, peak types (PGA, PGV, PGD), spectral characteristics (S_{aTs} , $S_{a1.5Ts}$, ASI),
104 and cumulative types (a_{sq} , v_{sq} , d_{sq} , a_{rs} , v_{rs} , d_{rs} , I_A , CAV, CAD, CAI, a_{rms} , v_{rms} , d_{rms} , I_c , t_d)—CAV
105 exhibited the highest correlation with the slope displacement response and more effectively captured
106 the characteristics of aftershocks (Zhang et al., 2024), as shown in Fig. 2. Consequently, CAV was
107 selected as the indicator for evaluating slope response under MAS.



108

109

Fig. 2. Correlation coefficient of the 21 ground motion parameters (Zhang et al., 2024)

110

Based on trial calculations, 96 sets of MAS were scaled to three CAV levels: 12 m/s, 28 m/s, and 40 m/s. Using the FLAC3D, the slope response under MAS, denoted as $\dot{X}_j(\theta_q, t); j=1, 2, \dots, 96$.

111

112

(3) Based on the above two steps to get assigned to probability P_q and slope of the response results $\dot{X}_j(\theta_q, t)$ probability density evolution Eq. (3):

113

$$\frac{\partial p_{X\theta}(x, \theta, t)}{\partial t} + \sum_{j=1}^m \dot{X}_j(\theta_q, t) \frac{\partial p_{X\theta}(x, \theta, t)}{\partial x} = 0, \quad q=1, 2, 3, \dots, 96 \quad (3)$$

114

115

Within this formulation, X designates system response quantities, θ encompasses the ensemble of random variables exclusive of initial conditions. $\theta = (X_0, \dot{\theta})$ represents the vector comprising all stochastic variables within the system; $X = H(\theta, t)$ indicates the physical response of X ; $p_{X\theta}(x, \theta, t)$ signifies the joint probability density function (PDF) for X and θ .

116

117

118

119

When $t = t_0$, the following initial condition is as shown in Eq. (4):

120

$$p_{X\theta}(x, \theta, t)|_{t=t_0} = \delta(x - x_0) P_\theta(\theta) \quad (4)$$

121

In this expression, δ denotes the Dirac delta function, while x_0 corresponds to the X value $t = t_0$. The PDF of X at any given time can be derived by accumulating all discrete numerical solutions, as expressed in Eq. (5):

122

123

124

$$p_X(x, t) = \int p_{X\theta}(x, \theta, t) d\theta \quad (5)$$

125

Probability density evolution equations necessitate numerical solution methodologies. Direct analytical solution derivation for Eq. (5). presents considerable mathematical complexity. Conventional practice employs finite difference approximations for solution advancement.

126

127

128

$$\frac{\partial p(z, t)}{\partial t} + a(t) \frac{\partial p(z, t)}{\partial z} = 0 \quad (6)$$

129

First-order Taylor series expansion of Eq. (6), yields approximate differential expressions:

130

$$\left[\frac{\partial p}{\partial t} \right]_j(k) = \frac{p_j^{(k+1)} - p_j^{(k)}}{\Delta t} \quad (7)$$

131

For spatial coordinate z , analogous treatment produces:

132

$$\left[\frac{\partial p}{\partial z} \right]_j(k) = \frac{p_j^{(k+1)} - p_j^{(k)}}{\Delta z} \quad (8)$$

133

Substitute Eqs. (7) and (8) into Eq. (6):



134
$$p_j^{(k+1)} = p_j^{(k)} - \lambda a^{(k)} [p_j^{(k)} - p_{j-1}^{(k)}] \text{ or } p_j^{(k+1)} = (1 - \lambda a^{(k)}) p_j^{(k)} + \lambda a^{(k)} p_{j-1}^{(k)} \quad (9)$$

135 Eq. (9) is the one-sided difference scheme. Substitute $\dot{X}_j(\theta, t)$ obtained from ② into Eq. (3),
136 and solve the partial differential equation using the L-W or TVD format of the finite difference
137 method.

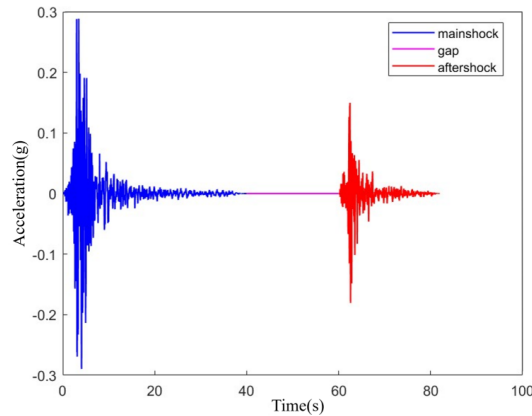
138 (4) The PDF of slope displacement response $p_X(x, t)$ is obtained numerically through
139 cumulative summation of the joint PDF $p_{X\theta}(x, \theta, t)$; $q = 1, 2, \dots, 96$. Subsequently, both PDF
140 and cumulative distribution function (CDF) graphs for slope displacement are developed. The
141 statistical characteristics of slope displacement datasets are visualized via these PDF and CDF
142 graphs to determine slope reliability.

143 3 Stochastic simulations of MAS

144 Empirical MAS recordings furnish superior fidelity representations of structural damage
145 phenomenology and cumulative degradation mechanisms (Yang et al., 2022). This study uses
146 diverse real seismic data to avoid bias from specific seismic motion types. Through iterative
147 parameter identification employing evolutionary power spectrum density modeling paradigms, this
148 study synthesizes theoretical frameworks with data-driven methodologies to construct stochastic
149 seismic input characterizations. This offers a stochastic loading source for studying how MAS affect
150 slope reliability.

151 This investigation selected 96 authentic mainshock-aftershock pairs from the Pacific Earthquake
152 Engineering Research Center strong-motion repository. Each MAS assembly adopted a "mainshock
153 + 20-second temporal gap + aftershock" configuration to preserve comprehensive non-stationary
154 sequence characteristics (Wang et al., 2023). Fig. 3 displays a typical mainshock-aftershock
155 acceleration record from the Whittier Narrows event, with the mainshock and aftershock numbered
156 589 and 707, respectively, in the NGA-West2 database.

157 For the mainshock-aftershock sequential ground motion assemblies constructed above,
158 frequency-domain energy distribution investigations proceed utilizing evolutionary power spectrum
159 modeling of fully non-stationary ground motion processes (Priestley, 1965; Liu et al., 2017). The
160 best square approximation criterion and the least square method are adopted to fit the energy
161 distribution curve in the frequency domain. The parameter vector λ is further obtained through
162 inversion and regression. In the process, considering the site damping ratio ξ_f excellence, site soil
163 circular frequency ω_f and the influence of a frequency modulation function parameter. The
164 identification results are shown in Fig. 4, and the data results are presented in Table 2. In the
165 constructed earthquake, it can be regarded as a zero-mean real non-stationary ground motion process
166 generated by the evolving power spectral density function model.



167

168

Fig. 3. Typical acceleration time history of a MAS

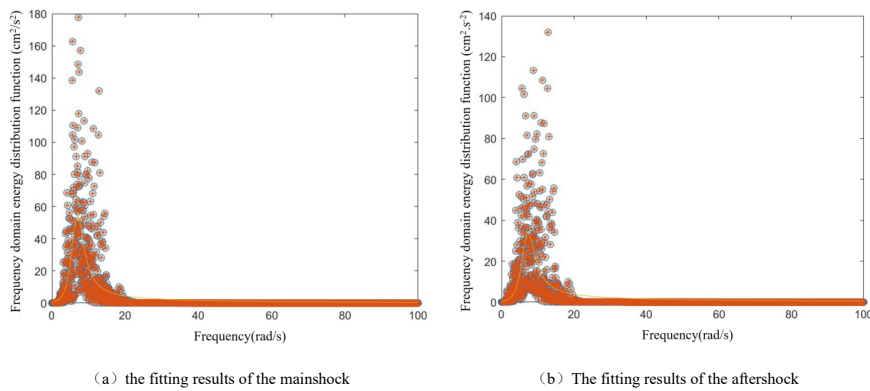


Fig. 4. The identification effect of the parameter vector λ

169

Table 2 Identification results of MAS

Earthquake type	Damping ratio	Superior circular frequency	Time-frequency modulation function
mainshock	0.32	14.09	0.64
aftershock	0.37	14.64	0.71

170

4 Results and analysis

171

172

173

174

175

176

177

178

179

180

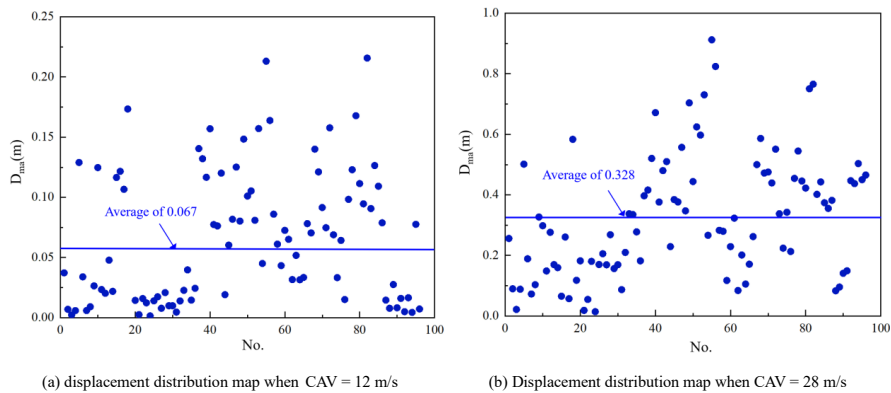
To assess slope reliability based on permanent displacement outcomes, defining critical stability states proves necessary. Jibson and Michael (2009) classified slope displacement into four ranges for seismic landslide risk evaluation: displacements of 0-1cm indicate low risk, 1-5cm suggest medium risk, 5-15cm represent high risk, and those exceeding 15cm denote very high risk. For permanent displacement, Yener (1988) suggests that the control standard for seismic sliding deformation is 1m. In this study, combined with the actual engineering requirements, three slope displacement thresholds of 0.05m, 0.5m and 1.0m were selected, corresponding to three failure degrees of low, medium and high respectively, to systematically evaluate the reliability of slope displacement under the MAS action.

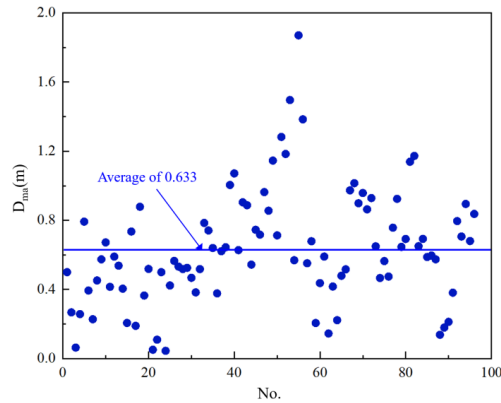
Fig. 5 shows the distribution of the slope permanent displacement under the MAS. The



181 distribution has a large degree of dispersion, and with the increase of ground motion intensity, the
182 displacement response of the slope also increases. When the CAV of the MAS was 12m/s, 28m/s
183 and 40m/s respectively, the permanent displacements of the slope were 0.067m, 0.328m and 0.633m
184 respectively, which were like the slope displacement results when the PGA of the MAS was 0.4g,
185 0.5g and 0.6g in reference (Wang et al., 2023). The difference is that the discreteness degree of the
186 permanent displacement of the slope obtained in this study becomes smaller. With the increase of
187 the CAV, the slope displacement response results are increasingly concentrated around the average
188 value. This tendency substantiates CAV superiority relative to PGA as the characterization
189 parameter for MAS when investigating slope displacement reliability.

190 Fig. 6 delineates PDF and CDF curves characterizing slope displacement. PDF curves reveal the
191 clustering patterns and variation extents within displacement datasets, thus presenting the
192 distributional features of slope movement data in a visual manner. The CDF curve determines the
193 cumulative probability of displacement and is used to evaluate the reliability of the permanent
194 displacement of the slope. The PDF for slope displacement shown in Fig. 5 display bimodal or
195 multimodal patterns, making it difficult to describe them using standard distributions like normal or
196 lognormal models. Under the MAS action of different intensities, the displacements of slopes have
197 diverse distribution patterns, and their probabilities are also not the same. When the CAV is 12 m/s,
198 the fluctuation span of slope displacement response ranges from 0-0.25m. Under a low failure
199 degree with a displacement threshold of 0.05 m, the reliability of the slope is 48.5%. With the growth
200 of CAV, the variation range of slope displacement response under the MAS keeps expanding, while
201 the concentrated area of permanent displacement becomes wider. When the CAV is 28 m/s, the
202 fluctuation span of slope displacement response extends from 0 m to 1 m, mainly concentrated
203 between 0 m - 0.5 m. Under the medium failure degree with the displacement threshold of 0.5 m,
204 the reliability of the slope is 82.0%. When the CAV is 40 m/s, the fluctuation span of slope
205 displacement response spans from 0 m to 2 m, mainly concentrated between 0 m -1 m. Under the
206 high failure degree with a displacement threshold of 1m, the slope's reliability reaches 91.7%.





(c) displacement distribution map when CAV = 40 m/s

Fig. 5. displacement response distribution of slopes under mas

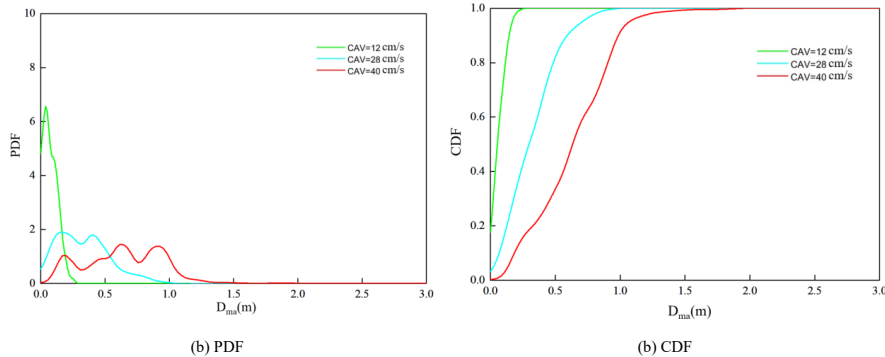


Fig. 6. Statistical analysis of slope displacement response probability under mas action

207 This investigation's outcomes undergo comparative evaluation against conventional slope
 208 displacement reliability analysis results, which customarily employ PGA as the seismic ground
 209 motion parameter (Wang et al., 2023), as depicted in Fig. 7-9. Fig. 7 demonstrates that the use of
 210 CAV as the seismic ground - motion parameter in this study leads to a more concentrated distribution
 211 of slope displacement. The range of displacement is reduced by 37.5% to 50%, the probability of
 212 outliers is lower, and the assessment of slope displacement response is more precise. Fig. 8 and Fig.
 213 9 indicate that at the low damage threshold of 0.05 m, the slope reliability is 39.2% when using PGA
 214 as the index, while it rises to 48.5% when using CAV as the index, showing an increase of 9.3%. At
 215 the moderate damage threshold of 0.5 m, the slope reliability is 76.7% for PGA and 82.0% for CAV,
 216 with an increase of 5.3%. At the high damage threshold of 1 m, the slope reliability is 77.2% for
 217 PGA and 91.7% for CAV, with an increase of 14.5%. These results demonstrate that using CAV as
 218 the seismic intensity control parameter for sequence-type ground motions can more effectively
 219 evaluate slope reliability.

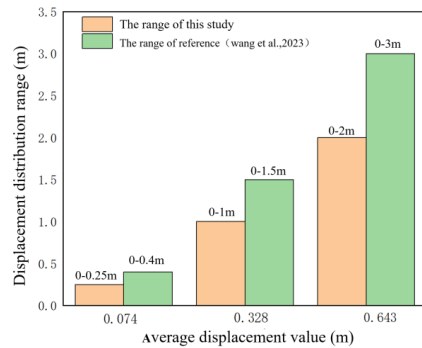


Fig. 7. Comparison of slope displacement response distribution

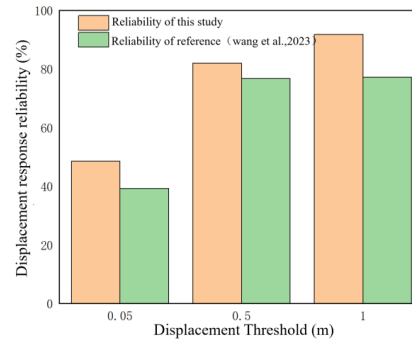


Fig. 8. Comparison of slope displacement reliability

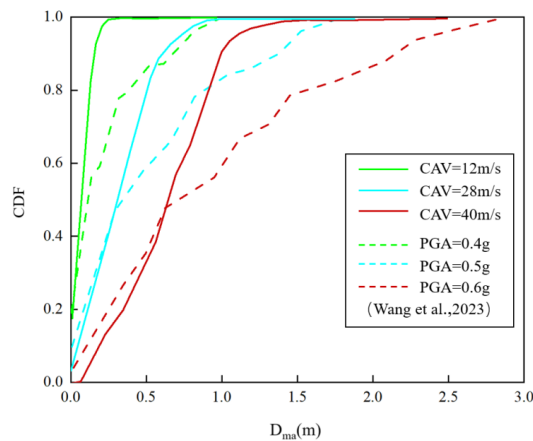


Fig. 9. Compared with the reliability results of slope displacement response in reference

220 5 Conclusions

221 By studying the intensity-controlling parameters of the MAS in soil slope responses and based
 222 on PDEM, an assessment methodology addressing slope reliability under MAS excitations is
 223 presented herein. Benchmarking against conventional techniques reveals the following insights:

224 (1) Among 21 distinct MAS parameter types, CAV demonstrates superior capability in capturing
 225 MAS characteristics and comprehensively representing MAS cumulative effects. Therefore, CAV
 226 can be used as the optimal parameter to assess the response of soil slopes under the MAS action.

227 (2) Based on the dynamic calculation results, as CAV increases from 12 m/s to 40 m/s, the slope
 228 displacement response gradually increases, while the displacement results still exhibit a degree of
 229 scatter. Consequently, employing probabilistic analysis methodologies becomes essential when
 230 evaluating soil slope stability under MAS loading.

231 (3) By incorporating MAS characteristics and utilizing PDEM, a methodology for computing
 232 slope displacement response reliability under MAS has been established. This method fully reflects
 233 the characteristics of aftershocks and can more accurately evaluate the response degree of slopes
 234 under MAS action, which has both theoretical significance and practical engineering value.



235 It is worth pointing out that this study focuses on clayey soil slopes in the southwestern region of
236 China, with an emphasis on the feasibility of the reliability analysis method for soil slope response
237 under MAS action. The study does not consider the variability of soil parameters. Considering the
238 variability of soil parameters will be of great significance to practical engineering applications.

239 *Code and data availability.* The MAS groundmotions in this study was based on the NGA-West2
240 strong-motion database from the Pacific Earthquake Engineering Research Center.

241 *Author contributions.* JZ and CZ designed the research and optimized the overall structure of
242 this paper. TW and CZ completed most of the main work, including the programming, debugging
243 of parameters, and final drafting of the article. SC and ZD contributed some important algorithm
244 ideas and completed the work of the comparison part. JZ and CZ provided the original algorithm
245 ideas and framework for this study and provides valuable suggestions for program optimization and
246 parameter adjustment.

247 *Competing interests.* The contact author has declared that none of the authors has any competing
248 interests.

249 *Disclaimer.* Views and opinions expressed are, however, those of the author(s) only and do not
250 necessarily reflect those of the European Union or REA. Neither the European Union nor the
251 granting authority can be held responsible for them.

252 *Publisher's note.* Copernicus Publications remains neutral with regard to jurisdictional claims
253 made in the text, published maps, institutional affiliations, or any other geographical representation
254 in this paper. While Copernicus Publications makes every effort to include appropriate place names,
255 the final responsibility lies with the authors. Views expressed in the text are those of the authors and
256 do not necessarily reflect the views of the publisher.

257

258 *Financial support.* This work was supported by the financial support from the National Natural
259 Science Foundation of China (Grant Nos. 51908176, 62273315 and 52192675). These financial
260 supports are gratefully acknowledged.

261

262 *Review statement.*

263 **References**

- 264 Amiri, S., Di Sarno, L., Garakaninezhad, A., 2022. Correlation between non-spectral and cumulative-based ground
265 motion intensity measures and demands of structures under mainshock-aftershock seismic sequences
266 considering the effects of incident angles. *Structures* 46, 1209–1223.
267 <https://doi.org/10.1016/j.istruc.2022.05.033>
- 268 Hu, C. B., Wang, Y. G., Ling, D. S., 2017. Physical essence and influence of model parameters on dynamic response
269 of Rayleigh damping. *J. Zhejiang Univ. (Eng. Sci.)* 51 (7), 1284 - 1290. <https://doi.org/10.3785/j.issn.1008-973X.2017.07.003>.
- 270
- 271 Hu, S., Gardoni, P., Xu, L., 2018. Stochastic procedure for the simulation of synthetic mainshock-aftershock ground
272 motion. *Earthquake Eng. Struct. Dyn.* 47 (11), 2275–2296. <https://doi.org/10.1002/eqe.3026>



- 273 Jiang, Y., Ruan, X., Liu, Z., 2021. Dimension-reduction simulation of main-aftershock type ground motion process.
274 J. Vib. Shock 40 (24), 282–292.
- 275 Jibson, R.W., Michael, J.A., 2009. Maps showing seismic landslide hazards in Anchorage, Alaska. Washington, DC:
276 USGS. <https://doi.org/10.1016/j.enggeo.2022.106853>
- 277 Li J, Chen J. The principle of preservation of probability and the generalized density evolution equation[J]. Structural
278 Safety, 2008, 30(1): 65-77.
- 279 Li, J., Chen, J., 2017. Some new advances in the probability density evolution method. Appl. Math. Mech. 38 (1),
280 32–43. <https://doi.org/10.1007/s10778-017-0084-2>
- 281 Li, J., Liu, Z., Chen, G., 2009. Orthogonal expansion of ground motion and PDEM-based seismic response analysis
282 of nonlinear structures. Earthq. Eng. Eng. Vibration 8, 313–328. <https://doi.org/10.1007/s11803-009-9090-8>
- 283 Li, S. H., Yang, S. P., 2006. Research status of hysteretic nonlinear models. J. Dyn. Control 4 (1), 8 - 15.
284 <https://doi.org/10.3969/j.issn.1672-6553.2006.01.003>.
- 285 Liu, Z., Jiang, Y., Liu, Z., Ruan, X., 2022. Dimension-reduction simulation of main-aftershock type vector process
286 based on strong motion records. Earthq. Eng. Eng. Dyn. 42 (4), 179–190.
287 <https://doi.org/10.13197/j.eeed.2022.0420>
- 288 Liu, Z., Liu, Z., 2017. Simulation of fully non-stationary ground motion based on seismic design response spectrum.
289 J. Vib. Eng. 30 (3), 457–465. (in Chinese)
- 290 Liu, Z., Liu, Z., Ruan, X., et al., 2019. POD-based dimension reduction representation of stochastic ground motion
291 fields. Sci. Sin. Technologica 49 (5), 589–601. (in Chinese)
- 292 Ma, Z. G., Zhu, B. L., Wu, H. G., et al., 2023. Experimental study on seismic failure characteristics optimization of
293 landslide - tunnel shock absorption based on energy analysis. Chin. J. Rock Mech. Eng. 42 (04), 879 - 895.
294 <https://doi.org/10.13722/j.cnki.jrme.2022.0516>.
- 295 Nithin, V. L., Das, S., Kaushik, H. B., 2020. Stochastic simulation of fully nonstationary aftershock ground motions
296 from known preceding mainshock. Soil Dyn. Earthq. Eng. 130, 1–11.
297 <https://doi.org/10.1016/j.soildyn.2020.105968>
- 298 Pang, R., Xu, B., Zhou, Y., et al., 2021. Seismic time-history response and system reliability analysis of slopes
299 considering uncertainty of multi-parameters and earthquake excitations. Comput. Geotech. 136, 104245.
300 <https://doi.org/10.1016/j.compgeo.2021.104245>
- 301 Pang, R., Yao, H., Xu, M., et al., 2024. Slope displacement reliability analysis considering rock parameters spatial
302 variability subjected to stochastic mainshock-aftershock earthquake. Reliab. Eng. Syst. Saf. 251, 110337.
303 <https://doi.org/10.1016/j.ress.2023.110337>
- 304 Priestley, M. B., 1965. Evolutionary spectra and non - stationary processes. J. R. Stat. Soc. Ser. B (Methodol.) 27
305 (2), 204 - 229.
- 306 Puthanpurayil, A. M., Lavan, O., Carr, A. J., et al., 2018. Application of local elasticity continuum damping models
307 in nonlinear dynamic analysis. Bull. Earthquake Eng. 16, 6365 - 6391. <https://doi.org/10.1007/s10518-018-0424-7>.
- 308
- 309 Qu, H. L., Hu, H. G., Zhang, J. J., Zhu, D. P., 2015. Dynamic response characteristics of anchor cable piles under
310 ground motion. China Earthq. Eng. J. 37 (02), 317 - 323. <https://doi.org/10.3969/j.issn.1000-0844.2015.02.0317>.
- 311
- 312 Ruiz-Garcia, J., Negrete-Manriquez, J. C., 2011. Evaluation of drift demands in existing steel frames under as-
313 recorded far-field and near-fault mainshock-aftershock seismic sequences. Eng. Struct. 33 (2), 621–634.
314 <https://doi.org/10.1016/j.engstruct.2010.12.006>
- 315 Wang, G., Pang, R., Yu, X., et al., 2023. Permanent displacement reliability analysis of soil slopes subjected to
316 mainshock-aftershock sequences. Comput. Geotech. 153, 105069.



- 317 <https://doi.org/10.1016/j.compgeo.2023.105069>
- 318 Wang, W., Li, D. Q., Liu, Y., et al., 2021. Influence of ground motion duration on the seismic performance of earth
319 slopes based on numerical analysis. *Soil Dyn. Earthq. Eng.* 143, 106595.
320 <https://doi.org/10.1016/j.soildyn.2021.106595>.
- 321 Xu, B., Wang, G., Pang, R., 2025. Dynamic reliability analysis of slopes considering material parameter spatial
322 variability under mainshock-aftershock sequences. *J. Civ. Environ. Eng.* (in Chinese)
- 323 Yan, Z. H., Zhang, S., Zhang, X. D., Zhang, L. P., 2011. Study of dynamic response of bedding rock slope under
324 earthquake and influence of ground motion parameters. *Chin. J. Rock Mech. Eng* 30 (S2), 3522 - 3528.
325 <https://doi.org/CNKI:SUN:YSLX.0.2011- S2 - 022>.
- 326 Yang, C. W., Zhang, L., Dong, L. J., et al., 2022. Research on the difference of dynamic responses between bedding
327 and toppling rock slopes based on shaking table test. *Chin. J. Rock Mech. Eng.* 41 (02), 271 - 281.
328 <https://doi.org/10.13722/j.cnki.jrme.2021.0168>.
- 329 Yang, C.W., Zhang, L., Dong, L.J., et al., 2022. Seismic response differences of favorable and reverse dipping rock
330 slopes based on shaking table tests. *J Rock Mech. Eng.* 41 (02), 271–281. [https://](https://doi.org/10.13722/j.cnki.jrme.2021.0168)
331 doi.org/10.13722/j.cnki.jrme.2021.0168.
- 332 Yener Ozkan, M., 1998. A review of considerations on seismic safety of embankments and earth and rock-fill dams.
333 *Soil Dyn. Earthq. Eng.* 17 (7-8), 439–458. <https://doi.org/10.1016/j.enggeo.2022.106853>
- 334 Zhang, C., Zhang, J., Chen, S., et al., 2024. Response characteristics of soil slope under mainshock–aftershock
335 sequences–type ground motions: Incremental damage effect, polarity effect, and correlation. *Soil Dyn. Earthq.*
336 *Eng.* 187, 108940. <https://doi.org/10.1016/j.soildyn.2023.108940>.
- 337 Zhou, H., Wang, G., Yu, X., Pang, R., 2023. Dynamic reliability analysis of layered slope considering soil spatial
338 variability subjected to mainshock-aftershock sequence. *Water* 15 (8), 1540.
339 <https://doi.org/10.3390/w15081540>